行政院國家科學委員會專題研究計畫 期中進度報告

發展動態顯影及具標定功能之生醫分子磁振影像: 評估肺癌之腫瘤生成、轉移、血管新生及治療反應--針對肺癌診斷與治療評估之核磁共振分子影像技術平台：具標定功能氧化鐵奈米粒子之發展(總計畫及子計畫二)(2/3)

期中進度報告(精簡版)

計 畫 類 別 ： 整合型
計 畫 編 號 ： NSC 96-2627-B-002-006-
執 行 期 間 ： 96 年 08 月 01 日至 97 年 07 月 31 日
執 行 單 位 ： 國立臺灣大學電機工程學系暨研究所

計 畫 主 持 人 ： 陳志宏
共 同 主 持 人 ： 袁昂、余忠仁、葉晨聖、吳育德

報 告 附 件 ： 出席國際會議研究心得報告及發表論文

處 理 方 式 ： 本計畫可公開查詢

中 華 民 國 97 年 06 月 04 日

行政院國家科學委員會補助專題研究計畫 □ 成 果 報 告 ■期中進度報告

（計畫名稱）

發展動態顯影及具標定功能之生醫分子磁振影像:評估肺癌之腫瘤生成、轉移、血管新生及治療反應(子計畫二)-針對肺癌診斷與治療評估之核磁共振分子影像技術平台：具標定功能氧化鐵奈米粒子之發展

Evaluation of tumorigenesis, metastasis, angiogenesis and therapeutic response of lung cancer in mice model with dynamic contrast perfusion MR Imaging and targeted MR molecular imaging (subproject 2)-The development and preparation of targeted Fe_3O_4 nanoparticles as MR contrast agent; its application for MR molecular imaging in lung cancer diagnosis and treatment

計畫類別：□ 個別型計畫　　■ 整合型計畫

計畫編號：NSC 95-2627-B-002-012

執行期間：96 年 8 月 1 日至 97 年 7 月 30 日

計畫主持人：陳志宏

共同主持人：袁昂、余中仁、葉晨聖

計畫參與人員：林韋廷、呂宜倩、蘇家豪

成果報告類型(依經費核定清單規定繳交)：■精簡報告　□完整報告

本成果報告包括以下應繳交之附件：

□赴國外出差或研習心得報告一份

□赴大陸地區出差或研習心得報告一份

■出席國際學術會議心得報告及發表之論文各一份

□國際合作研究計畫國外研究報告書一份

處理方式：除產學合作研究計畫、提升產業技術及人才培育研究計畫、列管計畫及下列情形者外，得立即公開查詢

□涉及專利或其他智慧財產權，□一年 ■二年後可公開查詢

執行單位：國立台灣大學

中　華　民　國　97　年　5　月　30　日

中、英文摘要及關鍵詞(keywords)

中文摘要

分子及活體細胞追蹤造影技術在臨床診斷與基礎醫學研究上扮演著日益重要的角色。本研究目的為發展生醫分子及活體細胞追蹤之磁振造影技術，並研究其在早期偵測並評估肺癌細胞小鼠模式之腫瘤血管新生型態功能及其轉移。主要內容為發展動態顯影磁振造影之血管新生評估技術、開發對細胞分子表現特異性鑑別之奈米磁振顯影劑、並且利用高溫超導射頻線圈及平行影像重建法來達到高訊雜比及高效率之磁振造影技術，用來研究肺癌細胞與肺臟轉移小鼠模式。結合上述技術之開發則可更進一步提供病灶分子病理資訊並設計多功能甚或智慧型藥劑，使醫師得以即時知道用藥之效能與投遞分布情形以最佳化治療策略。

此計畫針對肺癌之疾病模式作為主要之疾病研究標的，其主因為肺癌之臨床特徵為不易早期診斷，並常早期發生轉移，尤其是肺腺癌更常在疾病發現初期，即有遠處轉移之現象，並且常有手術後復發之情況。就目前的治療成效，非小細胞肺癌對放射線治療及化學治療之反應也較差。因此研究發展早期診斷肺癌、早期偵測肺癌轉移、評估腫瘤血管新生能力以及監測肺癌治療反應之新方法，即成為刻不容緩之課題。於此，本團隊已建立 VEGF(vascular permeability factors)與 EGFR 超表現或低表現之鼠肺癌活體模型之標準化誘導程序，可快速以正位手術移植法重現，將作為本研究標的。

於子計畫二針對細胞分子表現特異性鑑別之奈米磁振顯影劑的發展平台部份，可藉由測試修改奈米粒徑及表面化學以改良並強化其顯影效果並合成可控制均勻大小之正(胺基)或負電荷(梭基)表面之氧化鐵奈米粒作為負顯影劑之核心部分；根據過去的文獻報導，EFGR(Epidermal growth factor receptor)為一腫瘤生長激素表面受器，其功能可被抗 EGFR 抗體抑制(本團隊已可自融合瘤量產並純化此抗體)，因此並進一步連結抗腫瘤特異性表面抗原之單株抗體，如 EGFR 或其重組抗體，以作為融合標的投遞之導向器及攻擊武器於一體之雙功製劑。

為求有較高效率之對比試劑，於此計畫中亦同時發展新型態之釓奈米材料作為正向對比顯影，如此可增加多功能製劑的奈米載體，並作為發展新型顯影藥物之技術平台。

英文摘要

Molecular and cell specific imaging play increasingly important roles in both clinical diagnosis and fundamental biomedical researches. In this study, we aim to develop a platform of nanocontrast agents and molecular MR imaging system that specifically recognizes cancer cells and exerts its therapeutic efficacy while enables real-time tracking of the drug distribution. This kind of system will provide not only valuable molecular pathological information but also real-time therapeutic efficacy evaluation for personalized healthcare treatment strategy.

Among various disease models, lung cancer is one of the most common causes of cancer-related death in Taiwan (top 2nd) as well as other industrialized nations. The prognosis of lung cancer is poor as compared with other malignancies. Therefore, the research for early diagnosis, early detection of metastasis, and tumor-associated angiogenesis process, and assessment of therapeutic response become more and more important for lung cancer diagnosis and treatment. In this study, pulmonary tumor implantation animal models in mice with high and low VEGF (vascular permeability factors) and EGFR expression lung cancer cell carcinoma model were established by our team and will be used through the whole three years.

In subproject 2, there are evidences of non-invasive measurement of vascular permeability characteristics and apoptosis of tumor before the change of tumor size by using MRI with the information from apparent diffusion coefficient (ADC) and superparamagnetic iron oxide (SPIO) particles. For specifically recognized cancer cells, we have previously developed synthesis of iron oxide nanoparticles with excellent stability, biocompatibility, and interface for additional biochemical modifications. In this project, we will improve the synthesis and modifications of iron oxide nanoparticle to achieve better contrast and targeting effect. Furthermore, for combined molecular expression specific cancer targeting and therapy, bioconjugation of nanoparticles with anti-EGFR(Epidermal growth factor receptor) monoclonal antibody or specific recombinant ligand peptides will be performed, and the materials will be evaluated whether or not an increased signal contrast and hence high detection rate could be achieved for early detection of metastatic lesions.

Furthermore, we also developed Gd-based nanocontrast agents for MR positive contrast agent using in this year, and this Gd-based nanocontrast agent would be as platform for nanomedicine and photothermal therapy applications.

Keywords

Molecular imaging, Non-invasive, Lung cancer, Iron oxide nanoparticle, Anti-EGFR antibody, Gd-based nanocontrast agents, Nanomedicine.

前言、研究目的、文獻探討

Nanoparticle systems are promising new paradigms in pharmacotherapy and are being used in gene therapy, drug delivery,[1,2] imaging,[3,4] and novel drug discovery techniques.[5,6] The aim of nanodiagnostics is to identify disease at its earliest stage, particularly at the molecular level. Nanoparticle-based molecular imaging has set a unique platform for cellular tracking, targeted diagnostic studies, and image-monitored therapy.[7-10] Magnetic resonance imaging (MRI) has been recognized as the most important development in medical diagnosis since the discovery of the X-ray.

Despite significant progress in the understanding of molecular genetics of cancers, this malignant disease is still the top killer of human in many countries in the world. Early detection of cancer and its metastasis is important for the ultimate clinical outcome. Within a wide spectrum of medical imaging modalities, MRI offers a high spatial resolution, excellent depth of penetration with tomography capability, outstanding soft tissue contrast, and provides good anatomical detail and orientation. However, conventional MRI also suffered from the relatively low signal contrast as a result of partial-volume dilution effects.[11] Different image contrast agents have been developed for MRI through modulation of proton T_1 or T_2 relaxations using contrast agents such as Manganese (Mn^{2+}),[12] Gadolinium ethoxybenzyl diethylenetriamine pentaacetic acid (Gd-EOB-DTPA)[13] or iron oxide nanoparticles.[14] Iron oxide nanoparticles are in general biocompatible and provide excellent negative image contrast effect under T_2 or T_2* sequences. Iron oxides of various composition, size, shape and surface modifications have been developed and evaluated in the past decades for their MRI applications from laboratory to clinical usage.[15-18] However, *in vivo* molecular targeting imaging is still in the proof of concept stage.[19] Some pioneer works were performed in early nineties. Currently, MR contrast agents are categorized into T_1-positive agents of paramagnetic species, the Gd-based nanorods ($Gd(BDC)_{1.5}(H_2O)_2$ nanorods), where BDC denotes 1,4-benzenedicarboxylate embedded with Eu^{3+} or Tb^{3+} ions, were successfully synthesized using a reverse microemulsion method.[20] Those hybrid nanorods demonstrated the performance of MR and luminescent images, and the literatures pertaining to the inorganic Gd-based particles preparation and their further surface modification were seriously limited. Very recently, the bifunctional probes consisting of Gd_2O_3 nanoparticles conjugated with different fluorescent dyes (FITC, RBITC, or Cy5 NHS ester) were directly demonstrated *in vivo* studies.[21] On the other hand, the T_2-negative agents of superparamagnetic particles, the superparamagnetic particles (T_2-negative agents) are nano-sized or sub-micrometer-sized and are classified as superparamagnetic iron oxide (SPIO), ultrasmall SPIO (USPIO), or monocrystalline iron oxide nanoparticles (MION).[22,23] Superparamagnetic particles consist of many magnetic ions with significant, large, unpaired spins; they are superparamagnetic when the magnetic ions are mutually aligned.

Lung cancer is the most common cause of cancer-related death in Taiwan (top 2) and other industrialized nations. Therefore, the research for early diagnosis, early detection of metastasis, and

tumor-associated angiogenesis process, and assessment of therapeutic response become more and more important for lung cancer diagnosis and treatment. On the other hand, the epidermal growth factor receptor (EGFR) is a tyrosine kinase (TK) receptor of the ErbB family that is commonly altered in epithelial tumors. EGFR was shown to be an oncogene, capable of inducing cancer when aberrant and the EGFR was shown to be expressed in multiple cancer types at elevated levels relative to normal tissues.[24,25] Investigators demonstrated that use of specific monoclonal antibodies against the EGFR could inhibit its activity.[26] Since EGFR appeared to play a central role in tumorigenesis, this observation implied that targeting the receptor itself might be a useful way to detect and treat EGFR-expressing cancers. The epidermal growth factor receptor (EGFR) is detected by immunohistochemistry on up to 80% of non–small cell lung cancers (NSCLC)[27, 28]. Over-expression of EGFR in NSCLC is correlated with a high metastatic rate, poor tumor differentiation, and a high tumor growth rate[29, 30]. In this subproject, we developed magnetic nanoparticles MR probe conjugated to anti-EGFR (epidermal growth factor receptor) antibody, and we used these magnetic nanoparticles MR probe targeting the surface marker of non-small cell lung cancer cell to evaluate the usefulness of this molecular imaging technique in early detection of lung cancer and its metastasis, predict response to specific chemotherapy base on genomic changes, and assessment the response to multiple modalities of cancer therapy.

Therefore, the aims of this subproject in the second year are:

1. To use magnetic nanoparticle MR probes targeting wild type EGFR on non-small cell lung cancer cell and MR molecular imaging to assess their ability to detect tumor, or distant metastasis at early stage in SCID mice xenograft model.
2. To development Gd-based nanocontrast agents for MR molecular imaging.
3. To compare the molecular MR image signal changes indicating apoptosis with the degree of apoptosis revealed by TUNEL staining of the tumor specimens.

Reference

(1) Shaffer, C. *Drug Discov. Today* **2005**, *10*, 1581-1582.

(2) Vinogradov, S. *Expert. Opin. Drug Deliv.* **2004**, *1*, 181-184.

(3) Muldoon, L. L.; Tratnyek, P. G.; Jacobs, P. M.; Doolittle, N. D.; Christoforidis, G. A.; Frank, J. A.; Lindau, M.; Lockman, P. R.; Manninger, S. P.; Qiang, Y.; Spence, A. M.; Stupp, S. I.; Zhang, M.; Neuwelt, E. A. *AJNR Am. J. Neuroradiol.* **2006**, *27*, 715-721.

(4) Li, K. C.; Pandit, S. D.; Guccione, S.; Bednarski, M. D. *Biomed. Microdevices* **2004**, *6*, 113-116.

(5) Wilkinson, J. M. *Med. Device Technol.* **2003**, *14*, 29-31.

(6) Roco, M. C. *Curr. Opin. Biotechnol.* **2003**, *14*, 337-346.

(7) Winter, P. M.; Morawski, A. M.; Caruthers, S. D.; Fuhrhop, R. W.; Zhang, H.; Williams, T. A.; Allen, J. S.; Lacy, E. K.; Robertson, J. D.; Lanza, G. M.; Wickline, S. A. *Circulation* **2003**, *108*, 2270-2274.

(8) Krause, M. H.; Kwong, K. K.; Gragoudas, E. S.; Young, L. H. *Magn. Reson. Imaging* **2004**, *22*,

779-787.

(9) Bulte, J. W.; Zhang, S.; van Gelderen, P.; Herynek, V.; Jordan, E. K.; Duncan, I. D.; Frank, J. A. *Proc. Natl. Acad. Sci. U S A* **1999**, *96*, 15256-15261.

(10) Anderson, S. A.; Glod, J.; Arbab, A. S.; Noel, M.; Ashari, P.; Fine, H. A.; Frank, J. A. *Blood* **2005**, *105*, 420-425.

(11) Shapiro, E. M.; Sharer, K.; Skrtic, S.; Koretsky, A. P. *Magn. Reson. Med.* **2006**, 55, (2), 242-9.

(12) Lee, J. H.; Koretsky, A. P. *Curr. Pharm. Biotechnol.* **2004**, 5, (6), 529-37.

(13) Bluemke, D. A.; Sahani, D.; Amendola, M.; Balzer, T.; Breuer, J.; Brown, J. J.; Casalino, D. D.; Davis, P. L.; Francis, I. R.; Krinsky, G.; Lee, F. T., Jr.; Lu, D.; Paulson, E. K.; Schwartz, L. H.; Siegelman, E. S.; Small, W. C.; Weber, T. M.; Welber, A.; Shamsi, K. *Radiology* **2005**, 237, (1), 89-98.

(14) Nishimura, H.; Tanigawa, N.; Hiramatsu, M.; Tatsumi, Y.; Matsuki, M.; Narabayashi, I. *J. Am. Coll. Surg.* **2006**, 202, (4), 604-11.

(15) Cheng, F. Y.; Su, C. H.; Yang, Y. S.; Yeh, C. S.; Tsai, C. Y.; Wu, C. L.; Wu, M. T.; Shieh, D. B. *Biomaterials* **2005**, 26, (7), 729-38.

(16) Lee, H.; Lee, E.; Kim do, K.; Jang, N. K.; Jeong, Y. Y.; Jon, S. *J. Am. Chem. Soc.* **2006**, 128, (22), 7383-9.

(17) Muller, K.; Skepper, J. N.; Posfai, M.; Trivedi, R.; Howarth, S.; Corot, C.; Lancelot, E.; Thompson, P. W.; Brown, A. P.; Gillard, J. H. *Biomaterials* **2007**, 28, (9), 1629-42.

(18) Lencioni, R.; Bartolozzi, C. *Eur. Radiol.* **2004**, 14 Suppl 1, C10.

(19) Corot, C.; Robert, P.; Idee, J. M.; Port, M. *Adv. Drug Deliv. Rev.* **2006**, 58, (14), 1471-504.

(20) Rieter, W. J.; Taylor, K. M. L.; An, H.; Lin, W. *J. Am. Chem. Soc.* **2006**, *128*, 9024.

(21) Bridot, J. L.; Faure, A. C.; Laurent, S.; Rivière, C.; Billotey, C.; Hiba, B.; Janier, M.; Josserand, V.; Coll, J. L.; Vander Elst., L.; Muller, R.; Roux, S.; Perriat, P.; Tillement, O. *J. Am. Chem. Soc.* **2007**, *129*, 5076.

(22) Harisinghani, M. G.; Barentsz, J.; Hahn, P. F.; Deserno, W. M.; Tabatabaei, S.; van de Kaa, C. H.; de la Rosette, J.; Weissleder, R. *N. Engl. J. Med.* **2003**, *348*, 2491-2499.

(23) Shieh, D. B.; Cheng, F. Y.; Su, C. H.; Yeh, C. S.; Wu, M. T.; Wu, Y. N.; Tsai, C. Y.; Wu, C. L.; Chen, D. H.; Chou, C. H. *Biomaterials* **2005**, *26*, 7183-7191.

(24) Anderson, S. M.; Hayward, W. S.; Neel, B.G. et al. J. Virol. 1980, 36, 676-683.

(25) Nicholson, R. I.; Gee, J.M.; Harper, M. E. Eur. J. Cancer 2001, 37, S9-15.

(25) Gill, G. N.; Kawamoto, T.; Cochet, C. et al. J. Biol. Chem. 1984, 259, 7755-7760.

(27) Lynch, T. J.; Bell, D.W.; Sordella, R. et al. *N. Engl. J. Med.* **2004**, *350*, 2129–39.

(29) Amann, J.; Kalyankrishna, S.; Massion, P. P. et al. *Cancer Res.* **2005**, *65*, 226–35.

(30) a.) Herbst, R. S. *Int. J. Radiation Oncology Biol. Phy.* **2004**, *59*, 21–26; b.) Herbst, R. S. and Paul, A.

Bunn, Jr. *Cancer Res.* **2003**, *9*, 5813-5824.

研究方法

Second Year:

In this year, we assessed the ability of the EGFR-targeting MR molecular imaging to detect the subcutaneous transplanted tumor of different lung cancer cell lines *in vivo* in SCID xenograft model to evaluate the sensitivity of the EGFR-targeting MR molecular imaging to detect lung metastasis nodules *in vivo*. Furthermore, in the same way, we used magnetic nanoparticle MR probe targeting the mutated EGFR to assess the ability of MR molecular imaging to differentiate lung cancer with mutated EGFR or wild type EGFR. Furthermore, for the nanomedicine properties, we also developed the Gd-based nanocontrasr agents, and changed the composition by biocompatible polymer modification, then using for photothermal therapy.

The preparation of iron oxide nanoparticles

For preparing water-soluble and dispersed Fe_3O_4 nanoparticles, two-stage additions of protective agent and chemical co-precipitation were employed in the process. Briefly, two solutions containing Fe^{II} and Fe^{III} at pre-determined concentration ratio were mixed followed by addition of organic acid as adherent. Subsequently, the pH of the solution was carefully adjusted and proper amount of adherent was added to achieve complete coating of the particle surface that is required for Fe_3O_4 nanoparticle dispersion functionalized with $–NH_3^+$ group.

Electron micrographs of the magnetite dispersions were carried out using a drop of the sample onto a copper mesh coated with an amorphous carbon film, and then dried in a vacuum desiccator. The prepared samples were studied in a transmission electron microscopy (JEOL-JEM-1200-EX). The selected area electron diffraction patterns were recorded using a high resolution TEM (JEOL 3010 Analytical Scanning Transmission Electron Microscope) at an accelerating voltage of 200 kV.

Fe_3O_4 surface properties were characterized from both XPS and zeta potential measurements. The XPS spectra were recorded on an Omicron ultra high vacuum system, ESCA 2000-125. All XPS spectra were attained using a Mg Kα source (12 kV and 10 mA). The binding energy scale was calibrated to 284.6 eV for the main C 1s peak. The surface potential was measured by Zeta potential (Zetasizer 3000HS-Advanced).

The magnetization property of the nanoparticle was carried out at room temperature using a Quantum Design MPMS-7 SQUID magnetometer. The particle concentration was analyzed using an atomic absorption spectrometer (UNICAM Solaar M6 series), where the iron oxides were treated with nitric or hydrochloride acid until complete dissolution. Once the cationic iron concentrations were determined, the Fe_3O_4 nanoparticles concentrations were calculated on the basis of the average diameter of the iron oxide particles.

Hybridoma for monoclonal antibody production

Protein G-Sepharose, horseradish peroxidase (HRP)-conjugated goat anti-mouse IgG and HRP-conjugated donkey anti-rabbit IgG were purchased from Pierce Chemical (Rockford, IL); CNBr-activated Sepharose 4B was from Amersham Biotech Company (Uppsala, Sweden); FO cells were from the American Type Culture Collection (Rockville, MD); BALB/c mice, aged between 6 and 8 weeks, were from Nanjing University. All other reagents and chemicals were analytical grade.

Magnetic resonance nanoparticles coated with anti-EGFR or other antibodies

The modification of Fe_3O_4-NH_3^+ nanoparticles was used the traditional chemical cross-linking method. The iron oxide nanoparticle were reacted with antibody to form a covalent bond by catalyzing with 1-ethyl-3-(3-dimerthylaminopropyl)-car-bodiimide (EDC), and the molar ratio of Fe_3O_4-NH_3^+ nanoparticles and anti-EGFR antibody (or antibody against mutated EGFR, apoptotic marker, or endothelial cell marker), was 1 : 10.

Tumor cell lines

We chose three non-small cell lung cancer cell lines CL1-0, CL1-5, A549, lung cancer cell with mutated EGFR and one monocyte THP-1. All of them were cultured with ATCC complete growth medium RPMI 1640 medium within 2 mM L-glutamine, 1.5g/L sodium bicarbonate, 4.5 g/L glucose,100U/ml penicillin G sodium, 100μg/ml streptomycin sulfate and 10% fetal bovine serum in a humidified atmosphere consisting of 5% CO_2 in air at 37°C.

Tumor xenograft of NSCLC cell line CL1-5/A549 in SCID mice model

To assess tumorigenicity, 5 x 10^6 CL1-5, A549 lung cancer cells with EGFR overexpression confirmed by flow-cytomery were injected orthotopically into the subdermal region in the bilateral flanks of 4-to-6-week-old NOD SCID mice (Charles River, St. Constant, Quebec,Canada). Tumor volume (mm3) was estimated using the standard formula (length x width^2 x 0.5) per week after injection. We will use EGFR-targeting MR molecular imaging to image these tumor a different time points to determine the smallest size the MRI can detect these tumors.

Tumor will be resected after EGFR-targeting MR imaging, and the specimen will be stained for EGFR by IHC staining for comparison with the MR signal from EGFR-targeting MR imaging.

MRI for evaluation of primary tumor using EGFR-targeting magnetic nanoparticle MR probe

For evaluating the MR enhancement efficiency of Fe_3O_4 nanopartivles conjugated with anti-EGFR antibody, *in vivo* MR images were performed in the SCID mice model. The mice were anesthetized using isoflurane and then given Fe_3O_4 nanopartivles conjugated with anti-EGFR antibody (10 mg/kg), dispersed in normal saline, and injected *via* the jugular vein with a 30G-needle connected to the syringe with 100 cm polyethylene tubing. The MR experiments were acquired using a 3T Medspec/Biospec MRI system (Bruker, Ettlingen, Germany) with an inserted mini-gradient system, i.d. was 12 cm and a maximal gradient strength was 200 mT m^{-1}. A actively decoupled volume RF transmit coil with an inner diameter of 7.2 cm (Bruker BioSpin) was used for RF transmission, and a receive-only surface coil including low noise preamps (RAPID Biomedical) was used for RF reception. For the MR imaging, the coronal view had a field of view of 40 × 40 mm, a slice thickness of 1.5 mm, and a matrix size of 256 × 256, corresponding to the voxel size of 0.15 × 0.15 × 1.5 mm^3. T_2-weighted MR images were acquired using a fast spin echo imaging sequence with repetition time (TR) = 3500 ms, echo time (TE) = 62 ms, and the number of NEX was 8. T_2*-weighted MR images were acquired using a gradient echo imaging sequence with repetition time (TR) = 500 ms, echo time (TE) = 5.2 ms, flip angle (α) = 30^o and the number of NEX was 8.

Immunohistochemical staining of EGFR and evaluate of EGFR expression in tumor in SCID mice

Immunohistochemical staining was done on formalin-fixed, paraffin-embedded sections. Four- to 5-Am-thick sections were cut, deparaffinized in xylene, and rehydrated in graded alcohol. Antigen retrieval was done by boiling for 20 minutes in a microwave oven (Micro MED T/T Mega, 800 W) in a preheated 0.01 mol/L concentration of sodium citrate buffer (pH 6.0). Endogenous peroxidase activity was blocked by 3% hydrogen peroxide in ethanol for 5 minutes.

Slides were incubated for 1 hour with the mAb: 13 (1:10 dilution, Novocastra Laboratories, Newcastle upon Tyne, United Kingdom), or rabbit polyclonal antibody against survivin (1:100 dilution, NOVUS Biologicals, Littleton, CO). After the incubation, the slides were washed thrice with PBS and incubated for 30 minutes with MAX-PO (MULTI) secondary antibody mixture (Nichirei, Tokyo, Japan). After washing thrice with PBS, staining was done by incubation for 1 to 2 minutes with 3,3Vdiaminobenzidine used as the chromogen, and counterstaining was done with Myer's hematoxylin.

Synthesis of $Gd_2O(CO_3)_2 \cdot H_2O$ and Gd_2O_3 particles

For the synthesis of the $Gd_2O(CO_3)_2 \cdot H_2O$ spherical and rhombus-like particles, the typical preparation was performed by the addition of 1 mmol of urea (99%, Alfa Aesar) and 0.25 mmol of $GdCl_3 \cdot 6H_2O$ (99.5%, Aldrich) in 10 mL of distilled water with constant stirring for 10 min. Then the transparent solutions were maintained at 91 °C for a period of 4 (spheres) or 10 h (rhombus), leading to the formation of white precipitates. The white precipitates were collected by centrifugation and then washed three times with distilled water. This was followed by evaporation of the solvent in a vacuum desiccator for 4 h. The experimental parameter was also adjusted by the change of the concentration ratio of [urea]/[$GdCl_3 \cdot 6H_2O$] for the studies of the morphology affected. Table 1 lists the different experimental conditions and the resulting morphology. A calcination process (800 °C for 3 h with a rate of 4 °C/min) was performed to transform $Gd_2O(CO_3)_2 \cdot H_2O$ into white Gd_2O_3 crystalline. The morphologies were characterized by TEM (HITACHI transmission electron microscope), HRTEM (JEOL 2100 electron microscope) and SEM (JEOL JSM-6460 microscope) images. Infrared spectra were taken on a Nicolet Magana 550 FT-IR spectrophotometer. The crystalline of products was characterized by XRD (Rigaku D-Max IIIV diffractometer using Cu Kα radiation (λ = 1.5418 Å) at 30 kV and 30 mA).

Synthesis of Gd_2O_3/C nanoshells

We prepared a stock solvent by mixing isopropanol and toluene (v/v = 1/2 hereafter called "IT solvent") for the Gd_2O_3/C nanoshell experiments. The gelatins in ethanol were centrifuged and dispersed in IT solvent, called "IT gelatin solution". For Gd_2O_3/C preparation, 1 mL of IT gelatin solution was diluted by 9 mL of IT solvent. To prepare P123 solution, 1.62 g of P123 was added to 82.5 mL of ethanol containing 5.4 mL of 4.5 M HCl. The 0.075 mL of gadolinium(III) tris(isopropoxide) solution was then added to the diluted IT gelatin solutions (10 mL) and P123 solution (0.075 mL), and stirred for 3 h. The mixing solution (0.075 mL of gadolinium(III) tris(isopropoxide), 10 mL of diluted IT gelatin solutions, and 0.075 mL of P123 solution) was treated with hydrothermal process (hydrothermally heated in a sealed vessel at 88 ^oC for 14-16 h) in a temperature controlled oven. In the course of the hydrothermally heating, the hand-shaking action for the mixing solution was performed every 45 min for the initial 6-8 h, followed by aging for 7-8 h to form gelatin/inorganic composites. The composites were washed using IT solvent for five times. After drying in air, the composites were calcinated at 440 °C in air for 8 h leading to a black product. To obtain crystallized Gd_2O_3 with graphite carbon coating, an additional annealing process was operated for the black products at 600 ^oC under a N_2 atmosphere for 2h.

Synthesis of Gd_2O_3/C@PSMA nanoshells

A suspension solution of the Gd_2O_3/C@PSMA nanoshells was prepared by dispersing 2.5 mg of Gd_2O_3/C nanoshells into a 4 mL of PSMA aqueous solution (250 μg/mL PSMA and 0.25 M NaOH) via sonicating process in a sonication bath for an hour. The black Gd_2O_3/C@PSMA nanoshells were washed with deionized water and collected by centrifugation performance at 12000 rpm for 10 min.

Preparation of anti-EGFR conjugated Gd_2O_3/C@PSMA nanoshells

The Gd_2O_3/C@PSMA nanoshells (500 μg/mL) were incubated with anti-EGFR antibodies (25 μg/mL) in N-(2-hydrxyethyl)piperazine-N'-2-ethanesulfonic acid (HEPES) solution (pH 7.4). After 1 h incubation, the anti-EGFR conjugated Gd_2O_3/C@PSMA nanoshells were washed with phosphate-buffered saline (PBS, pH 7.4) solution and collected by a centrifugation/resuspension process at 4 ^oC, then stocked in the PBS buffer at 4 ^oC.

The biocompatibility of Gd-based nanocontrast agents

We treated a A549 (human epithelial lung cancer) cell line with various Gd-based nanomaterials and then used MTT (3-(4,5-dimethylthiazol-2-yl)-2,5-diphenyltetrazolium bromide) assay to determine the

biocompatibility of the nanoshells. The A549 cells were cultured in a 96-well microplate with Dulbecco Modification of Eagle medium (DMEM), plus 5% fetal bovine serum (FBS, Gem Cell). The cell density was 5×10^3 cells/well. The cells were maintained at 37 °C in a humid atmosphere of 95% air and 5% CO_2. After 24 h, serial diluents of Gd-based nanomaterials at concentrations of 500, 200, 100, 10, 1, 0.1, 0.01, 0.001, and 0 $\mu g/mL^{-1}$ were added to the culture wells to replace the original culture medium with a final volume of 100 μL. Subsequently, the cells were incubated with the particles for 24 h. The culture medium was then removed and replaced by 100 μL of fresh culture medium (DMEM) containing 10% MTT reagent for the MTT assay. The resulting cells were incubated at 37 °C for 4 h for the MTT assay to allow the formation of formazan dye. The cultural medium in each well was centrifuged (to prevent the nanoparticles from interfering with the spectrophotometric measurement) and transferred to an ELISA plate. The quantification determining cell viability was done using an ELISA plate reader at an optical absorbance of 540/650 nm.

Photothermal therapy of A549 cancer cells

A549 cancer cells were cultured in 96-well plates with Dulbecco Modification of Eagle medium (DMEM) plus 5% fetal bovine serum (FBS, Gem Cell) at 37 ^oC under 5% CO_2. Each well contained 5×10^4 cells for a culture time of 24h. The anti-EGFR conjugated Gd_2O_3/C@PSMA nanoshells was added to the cells and incubated for 1 h at 37 ^oC. To wash away the unbound anti-EGFR conjugated Gd_2O_3/C@PSMA, the experiment wells were rinsed with PBS buffer three times, then the fresh DMEM was added to each wells. The photothermal killing cancer cell was performed by using a CW diode laser with a wavelength of 808 nm with the beam spot of 1 mm^2. The cell viability was performed by staining the cells with calcein AM and ethidium homodimer-1 (EthD-1), giving green fluorescence for living cells and red fluorescence for dead cells.

成果與討論 (含結論與建議)

The preparation of iron oxide nanoparticles

In this subproject, we synthesized the Fe_3O_4 nanoparticles that modified with $-NH_3^+$ exhibit well-dispersed morphology last year, as shown in Fig. 1.

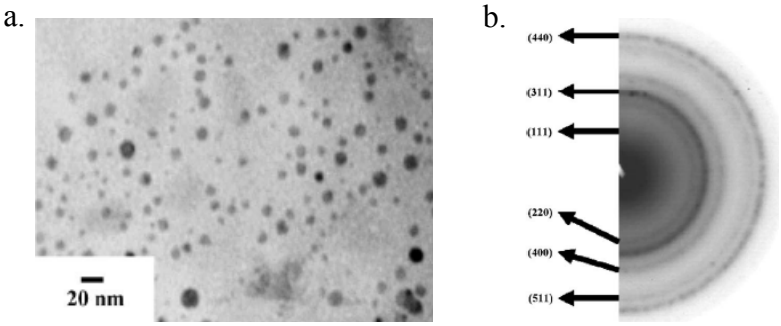

Figure 1. a.) TEM imaging showing Fe_3O_4 nanoparticles with average size of 6.2 ± 2.1 nm, and b.) Selected area electron diffraction pattern of the Fe_3O_4 nanoparticles.

Furthermore, for the targeting properties, we used anti-EGFR antibodies as a targeting model system to evaluate the strategy for covalent crosslinking of functional biomolecules and the targeting efficiency of various lung cancer cell lines and *in vivo* tumor targeting.

Immunohistochemical staining of EGFR and evaluate of EGFR expression in tumor in SCID mice

EGFR immunoreactivity was evaluated semiquantitatively according to the percentage of cells showing distinct cell membrane and/or diffuses cytoplasmic immunohistochemical reaction (Fig. 2). Cell menbrane and/or cytoplasmic immunoreactivities were assessed in at least five high-power fields at X400 magnification and assigned to one of the following categories: 0, <5%; 1, 5% to 20%; 2, >20%. Because tumors showed heterogeneous staining, the dominant pattern was used for scoring. A cutoff value of >20% was defined as a positive staining, and tumors with a score of 0 or 1 were considerednegative. The EGFR immunoreactivity also will be compared with the MR signal from EGFR-targeting MR imaging of the tumors.

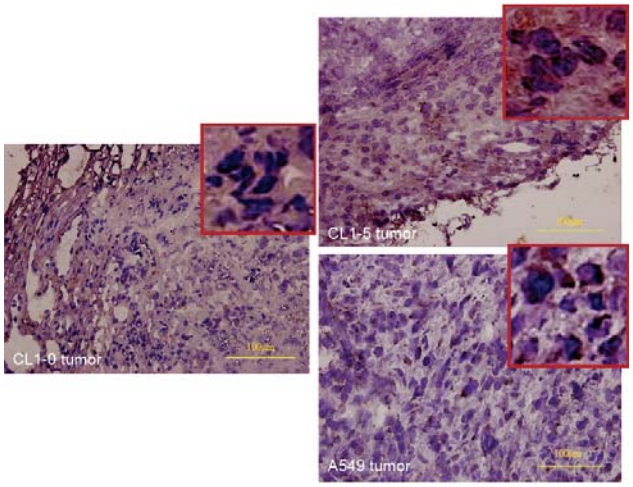

Figure 2. The immunohistochemical staining of EGFR in various tumor cell line in SCID mice. a.) CL 1-0 tumor, b.) CL 1-5 tumor;,and c.) A549 tumor.

In the Fig.2, the imaging of immunohistochemical staining showed that the expression of EGFR had different level in various tumor cell line. Herein, we found that the CL 1-5 and A549 have more EGFR expression on cell membranes of tumor section. Furthermore, we could apply the Fe_3O_4-anti EGFR antiboby nanocontrast agents for tumor region targeting in MR *in vivo* assay.

MRI for evaluation of primary tumor using EGFR-targeting magnetic nanoparticle MR probe

For MR *in vivo* assay, we used the 3 tesla superconductive scanner (ParaVison, Bruker, Germany) with a mini system including a resonator with active decoupling capability, animal bed for mice, and a 4-element array coil with integrated preamplifiers will be used to perform all MR studies.

Considering the MR contrast enhancement in T_2 and T_2* effect for iron oxide nanoparticles, in Fig. 3, the mice were administrated with Fe_3O_4 nanoparticles conjugated with anti-EGFR antibody (10 mg/Kg) *via* the jugular vein. We monitored the T_1-weighted imaging in a series imaging time at 3T MR system. Comparing with the tumor region, at post 3 h, the imaging of tumor (white arrow in Fig. 3) became slightly darker. After 6 h of circulation, we found that the tumor became darker that was enhanced by iron oxide nanoparticle targeting (shown in Fig. 3) appeared darker than pre-contrast images.

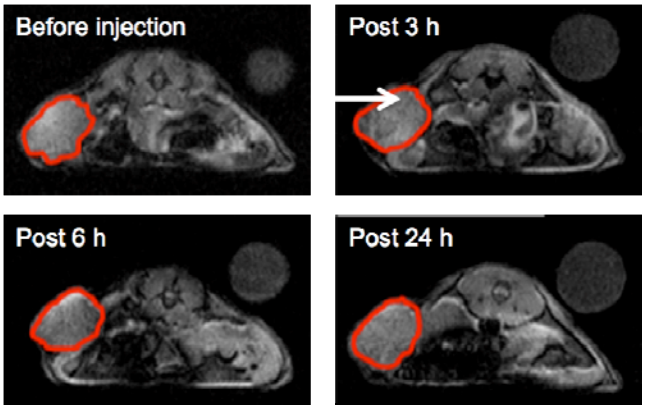

Figure 3. *In vivo* progressive MRI events. T_2*-weighted images of male SCID mice administrated with Fe_3O_4 nanoparticles conjugated with anti-EGFR antibody at the indicated temporal points (pre-injection, 3 h, 6 h and 24 h) (The white arrows indicate the tumor region).

Furthermore, we detected the signal intensity of tumor region from T_2*-weighted imaging (The red circled areas in Fig. 3 indicate the orthotopically induced tumor lesion), and showed in Fig. 4.

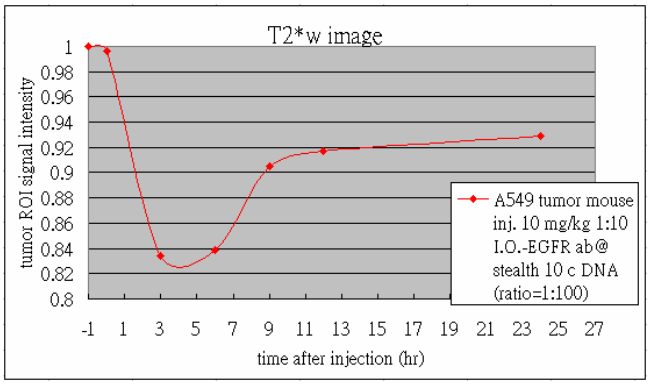

Figure 4. Modification of the magnetite nanoparticles with anti-EGFR antibody significantly decrease their absorption in the tumor region as revealed by quantitative measurement and compared to the time point before nanoparticle administration. (The red-circled areas in Fig. 3 indicate the tumor lesion)

As the result, we found that the signal intensity of tumor region could be enhancement by iron oxide nanoparticles that conjugated with anti-EGFR antibody in ca. 3~6 h, and the signal intensity of tumor region was decreased 17% after the mice were administrated negative nanocontrast agents. The signal contrast persisted for at least 12h after intravenous injection of the Fe_3O_4-anti-EGFR antibody nanoparticles.

To explore the tissue distribution of the Fe_3O_4-anti-EGFR antibody nanoparticles in the tumor and the organs, histological examine of formalin fixed paraffin embedded tumor and normal tissues was performed in the surgically removed specimens 24 hr after delivery of the nanoparticles. The tissues were sectioned at 5 μm thickness, processed for H&E or Pearl's iron stain then observed under a light microscopy (OLYMPUS BH-2, Japan) to reveal the tissue distribution of the aggregated iron oxide nanoparticles. As shown in Fig. 5, the tumor region (Fig. 5, H&E stain) presented a light bluish purple staining in iron stain

(Fig. 5, arrow head). On the other hand, we found that the liver and spleen would uptake the iron oxide nanoparticles, and showed the blue staining in histological examine (Fig. 5)

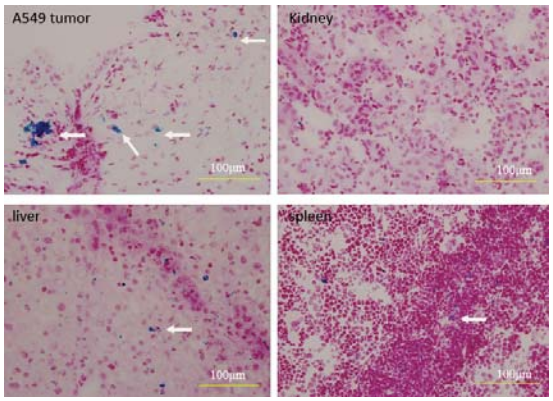

Figure 5. Lung cancer tissue and the organs of the same animal obtained 24h after i.v. injection of the Fe_3O_4-anti-EGFR antibody nanoparticles was processed for histological and histochemical analysis. Pearl's iron stain of the adjacent section showed a diffuse bluish purpose color (arrow head) in the tumor.

Preparations and Applications of $Gd_2O(CO_3)_2 \cdot H_2O$ and Gd_2O_3 particles for MR nanocontrast agents

The solution approach was employed to yield multifunctional amorphous $Gd_2O(CO_3)_2 \cdot H_2O$ colloidal spheres by a reflux of the aqueous solution containing $GdCl_3 \cdot 6H_2O$ and urea. By elongating the reaction time, crystalline rhombus-shaped $Gd_2O(CO_3)_2 \cdot H_2O$ with at least 87% yield could be formed and accompanied by some rectangular particles as well. The high resolution synchrotron powder X-ray diffraction have provided crystal structural information such as cell dimensions and indexed the exact crystal packing with hexagonal symmetry, which is absent from the JCPDS file, for crystalline rhombus sample. The particles formation was studied based on the reaction time and the concentration ratio of [urea]/[$GdCl_3 \cdot 6H_2O$]. After a calcination process, the amorphous spheres and crystalline rhombus $Gd_2O(CO_3)_2 \cdot H_2O$ particles converted into crystalline Gd_2O_3 at the temperature higher than 600 ^oC. For *in vitro* MR imaging, both $Gd_2O(CO_3)_2 \cdot H_2O$ and Gd_2O_3 species showed the promising T_1- and T_2-weighted effects and could potentially serve as bimodal T_1-positive and T_2-negative contrast agents. The amorphous $Gd_2O(CO_3)_2 \cdot H_2O$ contrast agent further demonstrated the enhanced contrast of the liver and kidney using a dynamic contrast-enhanced MR imaging (DCE-MRI) technique for *in vivo* investigation. The multifunctional capability of the amorphous $Gd_2O(CO_3)_2 \cdot H_2O$ spheres was also shown by the evidence of the formation of the nanoshell using amorphous spheres as the template particles. The surface engineering of the amorphous $Gd_2O(CO_3)_2 \cdot H_2O$ spheres could be performed by covalent bonding to form hollow silica nanoshells and hollow silica@Fe_3O_4 hybrid particles (shown in Scheme 1).

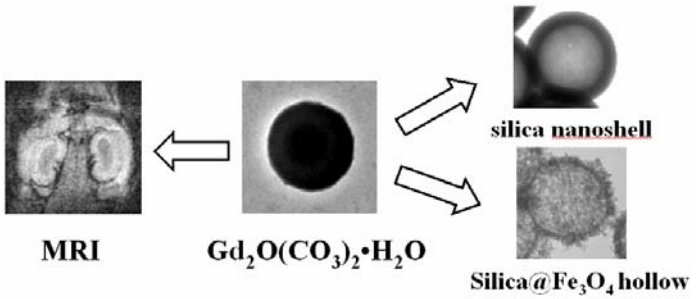

Scheme 1. The $Gd_2O(CO_3)_2 \cdot H_2O$ colloidal particles have been prepared by a reflux of the mixture containing $GdCl_3 \cdot 6H_2O$ and urea solution. The $Gd_2O(CO_3)_2 \cdot H_2O$ spherical particles exhibited multifunctional capability by the observation of showing MR contrast effect and serving as a template particle to fabricate silica hollow structures and to form composites with various nanoshell compositions.

The $Gd_2O(CO_3)_2 \cdot H_2O$ particles were synthesized by refluxing the aqueous solutions containing gadolinium salt and urea. In the preparation of the particles, the experimental parameters including the reaction time and the concentration ratio of [urea]/[$GdCl_3 \cdot 6H_2O$] were adjusted to study their effects on the particles formation. The formation of the sphere- and rhombus-shaped particles could be achieved by the change of the reaction time. Meanwhile, the increase of the [urea]/[$GdCl_3 \cdot 6H_2O$] ratio favors the polymorphs formation. Fig. 6a shows the spherical particles obtained exclusively from a ratio of [urea]/[$GdCl_3 \cdot 6H_2O$] = 4 (urea = 1 mmol ; $GdCl_3 \cdot 6H_2O$ = 0.25 mmol) for a reaction of 4 h at 91 ^oC.

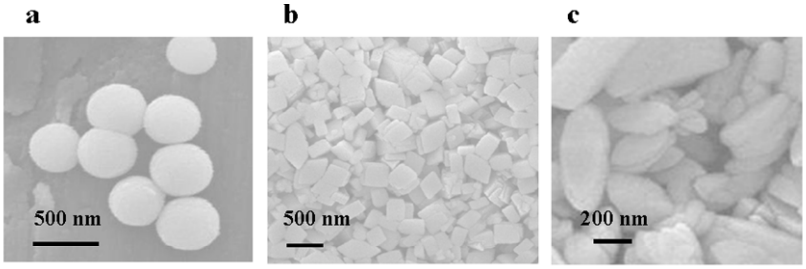

Figure 6. SEM images showing (a) the spherical particles obtained from a ratio of [urea]/[$GdCl_3 \cdot 6H_2O$] = 4 for a reaction of 4 h at 91 ^oC, (b) the rhombus-shaped particles obtained from a ratio of [urea]/[$GdCl_3 \cdot 6H_2O$] = 4 for a reaction for 10 h at 91 ^oC, and (c) the rice-shaped mixtures obtained from a ratio of [urea]/[$GdCl_3 \cdot 6H_2O$] = 8 for a reaction for 10 h at 91 ^oC.

Due to the potentially showing MR signal enhancement as contrast agents, these Gd-containing particles were evaluated for deleterious biological properties. The sphere and rhombus $Gd_2O(CO_3)_2 \cdot H_2O$ and cube-like Gd_2O_3 samples were chosen to verify their cytotoxicity. Cell viability experiments were conducted on a Vero cell line (monkey kidney cell line) using two well-established WST-1 and MTT assays. These particles were delivered over a range of dosages (0~200 μg/mL). Both assays showed satisfactory results for *in vitro* biocompatibility in all dosages for the particles, as seen in Fig. 7. Additionally, the leaching of

Gd^{3+} from the spherical $Gd_2O(CO_3)_2{\cdot}H_2O$ was examined in aqueous solution using xylenol orange as indicator for the detection of free Gd^{3+}. A very low free Gd^{3+} of ~23 μM leaching out from particles (with 2 mM of Gd^{3+}) was observed after 4 days incubation.

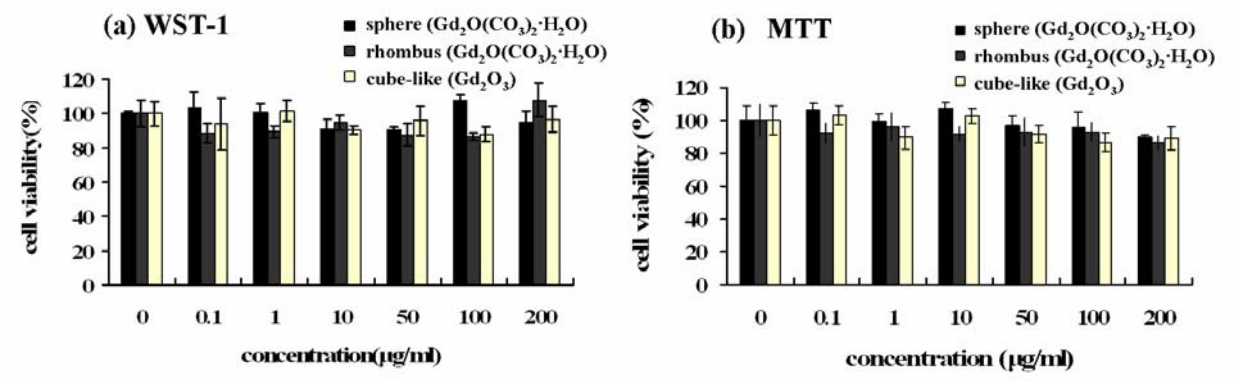

Figure 7. The biocompatibility of the sphere and rhombus $Gd_2O(CO_3)_2{\cdot}H_2O$ and cube-like Gd_2O_3 samples were analyzed using (a) WST-1 and (b) MTT assays. Vero cells were incubated with particles for 24 h.

Considering that the rhombus sample includes the rectangle shape, we have chosen the amorphous $Gd_2O(CO_3)_2{\cdot}H_2O$ sphere particles as an example to monitor the T_1 contrast enhancement in mice. The dynamic contrast-enhanced MR imaging (DCE-MRI) technique was introduced to trace the imaging effect of the $Gd_2O(CO_3)_2{\cdot}H_2O$ spheres. The T_1-weighted images were recorded every 12 sec for a total of 12 min and 48 sec period. We injected the $Gd_2O(CO_3)_2{\cdot}H_2O$ spheres (0.3 mg/kg) at 6^{th} repetition (at 61 sec) in the course of DCE-MRI imaging acquisition. In Fig. 8a, the DCE-MR imaging showed that the liver and kidney were apparently enhanced by $Gd_2O(CO_3)_2{\cdot}H_2O$ spheres starting from 10^{th} (post 48 sec) repetition acquisition. Fig. 8b displays that the signal intensity of liver and kidney were measured as compared with the signal of the background noise marked as green circle throughout the acquisition. It is apparent that the signal contrast of liver and kidney were enhanced at 10^{th} scan and remained brightness image up to 60^{th} (post 10 min 48 sec) repetition acquisition. In Fig. 8b, it shows that the increase of signal intensity of liver was consistent larger than that of kidneys and made the change of MR signal brighter in liver. Fig. 8c shows that the liver and the cortex of kidneys could be enhanced within 2 min 24 sec in T_1-weighted imaging. The evidence of the enhanced contrast in liver and kidney suggests that the amorphous $Gd_2O(CO_3)_2{\cdot}H_2O$ spheres could be introduced as an MR positive contrast agent.

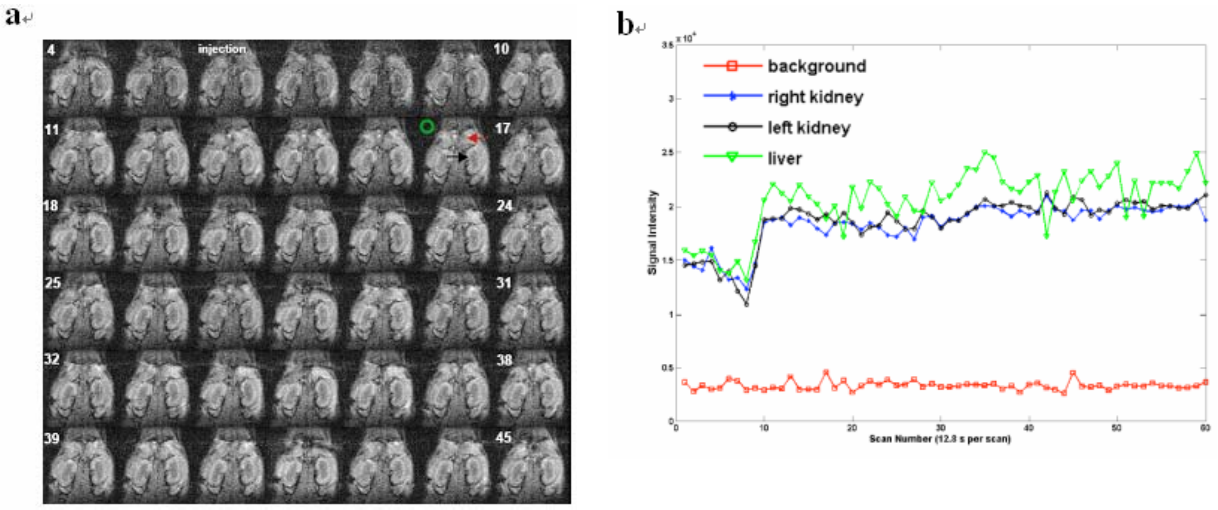

Figure 8. The dynamic contrast-enhanced MR imaging (DCE-MRI) of the $Gd_2O(CO_3)_2 \cdot H_2O$ (sphere-shaped particles). (a) The DCE-MR images from 4^{th} to 45^{th} repetition acquisitions that used gradient echo imaging sequence after injected particles (0.3 mg/kg) via retro-orbital plexus at 3T MR imaging system (red arrow: liver; black: kidney; green circle: region of interest of background). (b) The signal profile in liver area (red arrow) and kidney area (black arrow) as compared with the background noise (green circle).

The $Gd_2O(CO_3)_2 \cdot H_2O$ colloidal particles have been prepared by a reflux of the mixture containing $GdCl_3 \cdot 6H_2O$ and urea solution. In particular, the biocompatible amorphous $Gd_2O(CO_3)_2 \cdot H_2O$ spheres have been demonstrated showing T_1-enhancing and T_2-lowering effects, which provide an alternative choice for an MRI contrast agent. Furthermore, the ready surface modification has led to the $Gd_2O(CO_3)_2 \cdot H_2O$ spheres as an ideal template to form hollow nanoshells and hybrid composites. Based on the versatile combination strategy of the advantages of the surface engineering, MRI imaging and hollow structure shown by the $Gd_2O(CO_3)_2 \cdot H_2O$ spheres hold the great potential in developing innovative composite materials and multifunctional biomaterials with imaging, targeting, delivery, and therapeutic capabilities in one.

Preparations and Applications of Gd_2O_3/C nanoshells for MR nanocontrast agents

The dual function of Gd_2O_3/C nanoshells for the applications in the MR contrast images and NIR-triggered killing cancer cells. The surface of Gd_2O_3/C nanoshells could be readily modified by PSMA polymer to improve a water-dispersible property and promote their biocompatibility. The MR assays showed that Gd_2O_3/C and Gd_2O_3/C@PSMA nanoshells enhanced the image contrast in T_1-, T_2-, and T_2*-weighted images. Considering the different MR contrast enhancement for both nanoshells, the Gd_2O_3/C nanoshells were injected into BALB/C mice to monitor T_1 contrast and observed brightening images of kidneys cortex and liver. On the other hand, Gd_2O_3/C@PSMA nanoshells showed the live signal darkened in T_2 and T_2* contrast image. The generation of graphite carbon coated on Gd_2O_3 nanoshells display absorbance in the

near-infrared region. A large extinction coefficient of ε ~ 1563 $M^{-1}cm^{-1}$ at 808 nm was determined, indicating as a candidate for the potential photothermal agent. The Gd_2O_3/C@PSMA nanoshells conjugated with anti-EGFR antibodies were used for targeting and destroying A549 lung cancer cells. Both laser power density- and material dose-dependence were carried out to evaluate the photothermolysis in cancer cells.

SEM image (Fig. 9a) shows the products after 600 ^oC under N_2 as spherical particles. It can be seen that some of particles are broken (marked by black arrows), indicating the particle constructed of nanoshells structure with an interior cavity. The spherical nanoshells exhibit the average particle sizes of ~ 138 nm and shell thickness of ~ 19.2 nm (by counting 150 particles). Figure 9b shows X-ray diffraction (XRD) analysis of the nanoshell crystal structures before and after the addition of annealing process at 600 ^oC under N_2.

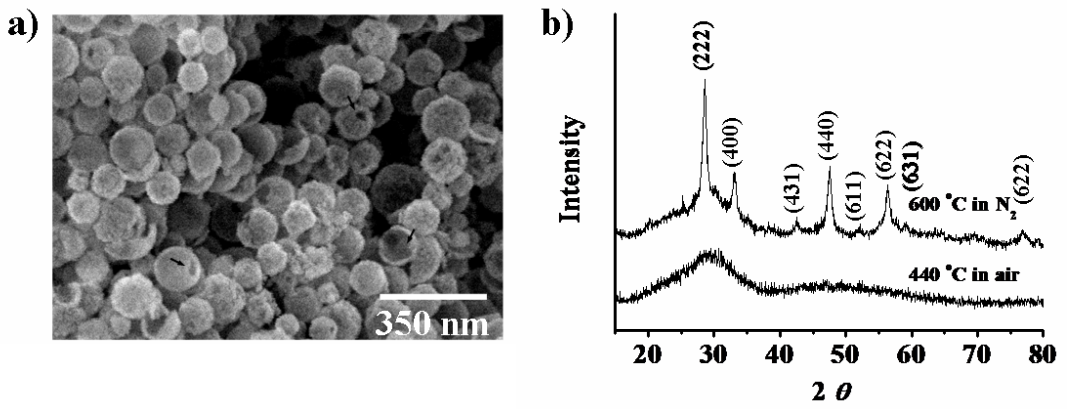

Figure 9. (a) SEM image of Gd_2O_3/C nanoshells prepared by a two-step thermal treatment: calcination at 440 ^oC in air, followed by annealing at 600 ^oC under N_2. (b) XRD patterns for the nanoshells prepared at 440 ^oC in air and at 600 ^oC in N_2.

For MR contrast agent applications, we evaluated the longtitudinal relaxation rate ($1/T_1$) and transverse relaxation rate ($1/T_2$) with various Gd ion concentrations of Gd_2O_3/C and Gd_2O_3/C@PSMA nanoshells (0 to 3.50 mM) in 5% agarose gel at 3T MR imaging system. The MR assays of T_1-, T_2-, and T_2*-weighted imaging show the imaging enhancement at various Gd ion concentrations of Gd_2O_3/C and Gd_2O_3/C@PSMA nanoshells (Fig. 10).

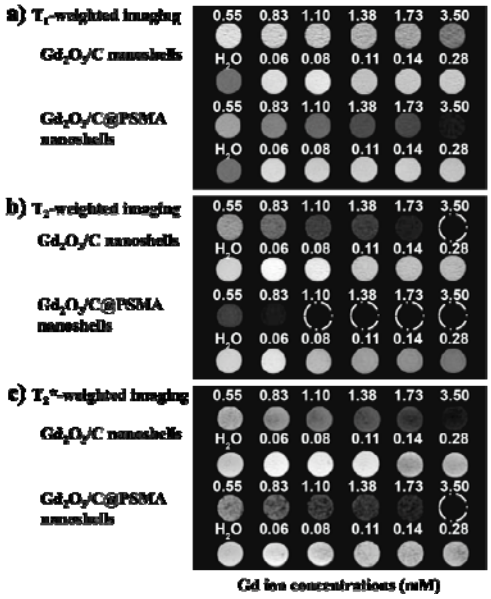

Figure 10. MR *in vitro* assays of Gd_2O_3/C and Gd_2O_3/C@PSMA (a) T_1-weighted images (repetition-time/echo-time (TR/TE) = 472 ms/9.4 ms), (b) T_2-weighted (TR/TE = 4500 ms/65 ms), and (c) T2*-weighted images (TR/TE = 500 ms/5.2 ms; flip angle ( ) = 30^o of nanoshells in water containing 0.5% agarose gel. The images were taken using the designed sequences with a matrix size of 256 × 192, a field of view of 60 × 60 mm, and a slice thickness of 6 mm operated at 125.3 MHz (3T MR system).

One malignant humanized lung cancer cell line, A549, which overexpresses the epithermal growth factor receptor (EGFR) on cell surface, was used to study the photothermal killing effect of Gd_2O_3/C@PSMA nanoshells. To highly specifically targeting to the A549 cancer cells, the anti-EGFR antibodies (humanized anti-EGF receptor (EGFR) antibody) were used to conjugate with Gd_2O_3/C@PSMA nanoshells. The laser irradiation power densities were varied from 5 to 35 W/cm^2 with a 7 min of irradiation to evaluate the cancer cells killing efficiency. The concentration of Gd_2O_3/C@PSMA nanoshells was fixed at 500 μg/mL. After NIR laser treatment, the cells were incubated with fluorescent labels of calcein AM and EthD-1 dyes, providing green emission for viable cells and red color for the dead cells, respectively. Fluorescence microscopy was employed to monitor images to observe cell viability. It was found that a significant loss of viability, with the area lacking green fluorescence (left) and exhibiting red fluorescence (right), began at 15 W/cm^2, as seem in Fig. 11a (middle row). On the other hand, cells remaining alive (a full green color image (left) and colorless image (right)) were observed as power density down to 10 W/cm^2 (Fig. 11a (bottom row)). This clearly demonstrated that the anti-EGFR conjugated Gd_2O_3/C@PSMA nanoshells could specifically target to EGFR overexpressed A549 cells and provided an effective locally heating to destroy the cancer cells upon exposing to 808 nm NIR light. Interestingly, we found that nanoshell dosage also affected photothermal killing effect. The nanoshells dose-dependent experiments were conducted and carried out at a fixed 20 W/cm^2 (Fig. 11b). The nanoshell dosage to cause cell death started at 400 μg/mL.

By dropping dosage to 300 μg/mL, there is not enough to cause cell death (high laser power required to induce cell demage).

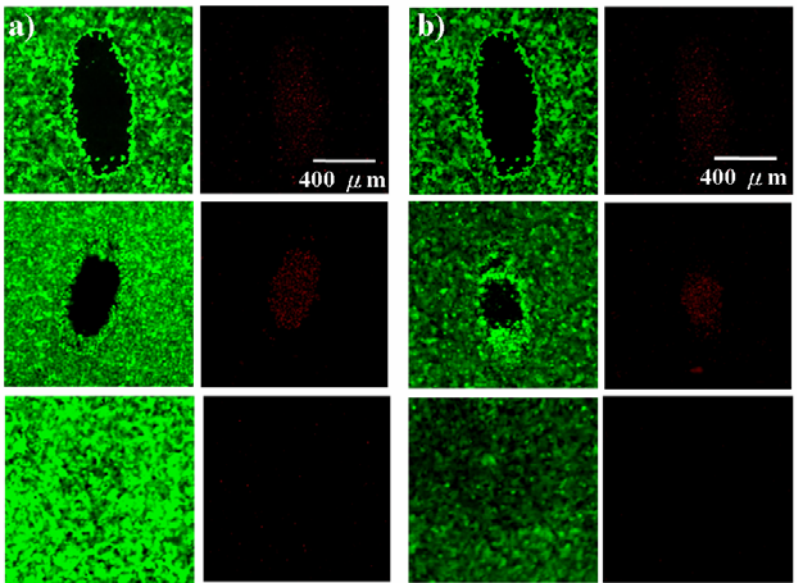

Figure 11. (a) Anti-EGFR conjugated with Gd_2O_3/C@PSMA nanoshells (500 μg/mL) treated with A549 cancer cells were irradiated by the laser dosages of 20 W/cm^2 (top row), 15 W/cm^2 (middle row), and 10 W/cm^2 (bottom row) for 7 min. (b) Anti-EGFR conjugated with Gd_2O_3/C@PSMA nanoshells were irradiated by the laser dosages of 20 W/cm^2 as a function of nanoshell dosages: 500 μg/mL (top row), 400 μg/mL (middle row), and 300 μg/mL (bottom row). The column shows staining by green fluorescence dye, calcein AM, for living cells. The column displays stainning by EthD-1, where the red fluorescence color indicates cell death.

We have presented the first report of Gd_2O_3/C@PSMA nanoshells showing bifunctionalities with efficient in MR anatomic imaging enhancement and photothermolysis of killing cancer cells. Interestingly, the MR assays show that we could switch the imaging contrast effect from positive Gd_2O_3/C contrast agents to negative Gd_2O_3/C@PSMA contrast agents. Cytotoxicity assay shows that the Gd_2O_3/C and Gd_2O_3/C@PSMA nanoshells have no significant toxicity and biodistribution indicates that they can be eliminated after 24 h. The graphite carbon coating on Gd_2O_3 nanoshells display large extinction coefficient of $\varepsilon \sim 1563$ $M^{-1}cm^{-1}$ at 808 nm with good absorbance in the near-infrared (NIR) region. Therefore, Gd_2O_3/C@PSMA nanoshells could act as promising photothermal therapeutic agent. By the oppositely charged interaction between Gd_2O_3/C@PSMA nanoshells and anti-EGFR antibodies, the antibody conjugated nanoshells could effectively target to malignant A549 lung cancer cells and exhibited therapeutic effect of killing A549 cells by photothermolysis.

計畫成果自評部份

In this year, we plan to build the platform of iron oxide nanoparticles and biocojugation of specific antibodies in NSCLC cell targeting and applied these nanocontrast agents in tumor targeting for *in vivo* MR molecular imaging. Furthermore, we plan to have Gd-based nanocontrast agents for positive contrast enhancement and kill the lung cancer cell (A549) by photothermal methodology. Up to date, the progress of this grant is under control, and we scale new heights in nanocontrast agents' development. Herein, we have completed the bioconjucation and modification of iron oxide nanoparticles, *in vivo* tumor targeting assay, and *in vivo* MR molecular imaging of tumor xenograft of NSCLC cell line A549 in SCID mice model.

As the results, we completed all of the goals in developments and applications of iron oxide nanocontrast agents for lung cancer targeting. Although the signal intensity was contrasted down by iron oxide nanoparticle in 17 %, we plan to change the modification strategy to increase the targeting efficiency. Furthermore, we also developed the Gd-based nanomedicine for MR contrast application and phototheemal therapy. In conclution, we achieved 100% of scheduled progress in subproject 2 in the second year.

Herein, these results of Gd-based nanomedicien were published on *Adv. Funct. Materials*. Furthermore, we also applied of iron oxide nanoparticle for oral cancer targeting and MR molecular imaging eveluation, and these results were published on *Bioconjugated Chem.* In brief, 2 abstracts have been represented in 6th Annual Meeting of Society of Molecular Imaging and 4 articles have been published. (shown in Table 1)

Table 1. The statistical table of publications in this integrated research project (2007/8 to 2008/5)

	2007	2008
Journal paper	**-**	**4**
Conference paper	**2**	**-**

With the support of this grant, one master student will be graduated this year, another Ph.D. student and master student work on further parallel imaging study and might graduate next year.

Publication

1. Chi-Chia Huang, Tzu-Yu Liu, Chia-Hao Su, Yi-Wei Lo, Jyh-Horng Chen, Chen-Sheng Yeh, "Superparamagnetic Hollow and Paramagnetic Porous Gd_2O_3 Particles", *Chem. Mater.* **2008**, Accepted. (IF: 5.104)
2. Fong-Yu Cheng, Saprina Ping-Hsien Wang, Chia-Hao Su, Tsung-Liu Tsai, Ping-Ching Wu, Dar-Bin Shieh, Jyh-Horng Chen, Patrick Ching-Ho Hsieh, and Chen-Sheng Yeh, "Stabilizer-free poly(lactide-co-glycolide) nanoparticles for multimodal biomedical probes", *Biomaterials*, **2008**, 29, 2104-2112. (IF: 5.196; 1/14)

3. I-Fang Li, Chia-Hao Su, Hwo-Shuenn Sheu, Hui-Chi Chiu, Yi-Wei Lo, Wei-Ting Lin, Jyh-Horng Chen, and Chen-Sheng Yeh, "The $Gd_2O(CO_3)_2 \cdot H_2O$ Particles and their Corresponding Gd_2O_3: Preparation and Applications of MR Contrast Agents and Template Particles for Hollow Spheres and Hybrid Composites", *Adv. Funct. Mater.* **2008**, *18*, 766-776. (IF: 6.779; 7/176)
4. Chien Yuan Lin, Chen Chang, Jyh Horng Chen, Tien Nan Lin " Dynamic Changes in Vascular Permeability, Cerebral Blood Volume, Vascular Density and Size after Transient Focal Cerebral Ischemia in Rats: Evaluation with Contrast-Enhanced Magnetic Resonance Imaging" *J. Cereb. Blood Flow Metab.*, ***2008***. Accepted. (IF: 4.843; 34/200)
5. Chia-Hao Su, Jun-Cheng Weng, Dar-Bin Shieh, Jyh-Horng Chen, Chen-Sheng Yeh, " The Novel Platform of Nanomedicine: For Drug Carrier and MR Contrast Agents Applications " *The 6th Annual Meeting of The Society for Molecular Imaging*, Rhode Island, American, **2007**.
6. Chia-Hao Su, Hwo-Shuenn Sheu, Chia-Yun Lin, Chih-Chia Huang, Yi-Wei Lo, Ying-Chih Pu, Jun-Cheng Weng, Dar-Bin Shieh, Jyh-Horng Chen, and Chen-Sheng Yeh, "Nanoshell Magnetic Resonance Imaging Contrast Agents" *2007 International Microprocesses and Nanotechnology Conference, No. 139,* Kyoto, Japan, **2007**.

出席國際學術會議心得報告

計畫編號	NSC 95-2627-B-002-012
計畫名稱	發展動態顯影及具標定功能之生醫分子磁振影像:評估肺癌之腫瘤生成、轉移、血管新生及治療反應
出國人員姓名 服務機關及職稱	陳志宏 服務機關：國立台灣大學 電機系　職稱：教授
會議時間地點	Sep. 7-11, 2007, Providence, Rhode Island, USA
會議名稱	Molecular Imaging Conference 2007
發表論文題目	The Novel Platform of Nanomedicine: For Drug Carrier and MR Contrast Agents Applications

一、參加會議經過

分子影像是處在生醫及物理科學的界面，且其快速地發展成一個重要的技術平台，在未來的醫學診斷及治療上，以及在藥物發現及開發上的重大突破，都將扮演一個中樞的角色。目前大多數的影像工具提供組織的結構及分析資訊，然而該領域的發展已經導致新影像工具的產生，目前它能夠讓研究人員洞悉機能性及分子的細節。為了包括生物學家、化學家、物理學家、電機工程師、電腦科學家及臨床科學家之跨領域研究。其中，為達成跨領域的目的，The Society of Molecular Imaging (SMI)與Academy of Molecular Imaging (AMI)合併於美國羅德島舉行2007分子影像國際會議。

此次赴美參加2007分子影像國際會議，主要是由於國內對於生醫分子影像之研究也正如火如荼地進行，且本人目前負責台大生醫分子影像中心，因此希望在生物探針MRI及光學影像方面可以於參加此一國際會議獲得更廣泛的研究觸角。

與會期間與多位從事分子影像的國際學者有深入的研究知識交流，且也由於SMI與AMI的整合與規劃下，其研究的領域已由基礎學理及應用跨足至臨床醫學的應用範疇。且研究方向大致可以分成下列幾項：（1）光學影像；（2）影像處理及管理；（3）使用磁性共振的小動物影像；（4）化學/生物探針的開發。上述的技術平台將被使用來支援的研究領域如癌症、新陳代謝及再生醫療。

二、與會心得

經由此一國際會議的參與，可以很明顯的發現分子影像的研究範疇已逐漸地擴大並有部分以進入臨床研究的階段。且亦由於奈米藥物的發展，對於標定性功能影像的研究也逐漸增加。並由此可以預見分子影像的研究在未來數年之間，是一相當重要且活躍的跨領域研究。但由於目前國內研究環境對於此一領域仍缺乏校際間的整合，且除本人所負責台大生醫分子影像核心實驗室外，仍無一相當之整合型研究團隊。有鑑於此，政府與學校單位應大力推動跨領域之生醫分子影像中心或重點發展研究領的培植與支援，冀以未來國內相關研究領域可於國際間有獨特發展與相互競爭的實力。